An Adaptive Control Allocation Algorithm for Nonlinear Vehicles with Parameter Uncertainty

Dong-liang Chen[1] and Guo-ping Liu[2]

***Abstract*— In this paper, an adaptive control allocation algorithm is proposed for nonlinear autonomous vehicles. Parameter uncertainty of effectors is considered in the design of allocation algorithm. By designing a nonlinear parameter estimator, it needs not to measure the control moments, i.e., forces and torques. Sensors and corresponding supporting devices to measure and transit the control moments are not needed, thus the overall cost of the control system is reduced, and the hardware system is simplified in implementation. Stability of the overall system is analyzed utilizing the Lyapunov method and sufficient conditions are derived. Digital simulation based on a spacecraft simulator is implemented. The results of the simulation validate the effectiveness of the control scheme.**

I. INTRODUCTION

For over-actuated systems, which have more actuators then the Degree of freedom, how to distribute the required control moment to the redundant actuators leads to the control allocation problem. Preliminaries and available solutions for this problem can be found in [6].

The control allocation for plants with nonlinear effectors is investigated in [8] [9], which employs a nonlinear programming method developed from sequential quadratic programming method. Optimal control allocation is adopted incorporating load information feedback to reduce structural load for aircrafts in [1] and [4]. Adaptive control allocation algorithm when the actuators are in failure are designed in [3] and [2] in conjunction with fault detection algorithms.

According to surveys, the control allocation for effectors with static parameters has been well studied, but little attention has been paid to control allocation problem for effectors with uncertain parameters. The uncertainty/variation of the parameters may cause bias even instability of the system. An inner-loop controller can mitigate the negative effects when the control moment, i.e. forces and torques, are measurable. But the measurement of control moments needs auxiliary sensors and devices, thus increases the complexity and cost of the system. Therefore the control moments may not be available in control allocation design in practice. As a result, advanced control allocation algorithm is in need to guarantee the stability of the system and improve the control performance.

*This work was supported in part by the National Natural Science Foundation of China under Grants 61333003 and 61690212 and the Short-term Oversea Visiting Project of Harbin Institute of Technology.

[1]Dong-liang Chen is with Department of Control Science and Engineering, Harbin Institute of Technology, Harbin 150001, China 13B904014@hit.edu.cn

[2] Guo-Ping Liu is with the School of Engineering, University of South Wales, Pontypridd CF37 1DL, UK and also with CT-GT center, Harbin Institute of Technology, Harbin 150001, China guoping.liu@southwales.ac.uk

In this paper, a novel control allocation scheme is proposed, where a nonlinear estimator is designed. The proposed control allocation algorithm is tested by digital simulation of a spacecraft simulator. The results of the digital simulation validate the effectiveness of the control allocation algorithm.

The main contributions of this paper include : an adaptive control allocation algorithm is designed, which mitigates the negative impacts brought in by parameter uncertainty/variation of the effectors without measurement of the control moment. Furthermore it guarantees that the solution asymptotically converges to the optimal trajectory.

II. PROBLEM FORMULATION

The nonlinear autonomous vehicles considered in this paper take the form of

$$\dot{x} = f(x,t) + G(\theta)u \tag{1}$$

where $x \in R^n$ is the state of the nonlinear plant, $f : R^n \times [0,\infty) \to R^n$ is a Lipschitz nonlinear function, and $f(0,t) = 0$, $G(\theta) \in R^{n\times m}$ is a function of the unknown parameter vector θ of the actuators, $\theta \in \Theta = \{v|v \in R^m\}$ with Θ the set of parameter vectors, $u \in R^m$ is control input of the actuator, the second term in right-hand side of (1) represents the control moment τ, that is

$$\tau = G(\theta)u \tag{2}$$

.

$m > n$ makes (1) an over-actuated system according to the definition.

Since $f(x)$ is a general nonlinear function, many vehicles can be expressed in the form of (1), such as spacecrafts, marine crafts, and etc. To simplify the theoretical analysis of the parameter uncertainty, a linear algebraic model is chosen to model the effectors. This is true when the nonlinearity of the vehicles can be neglected.

θ is the parameter vector of the actuators. In practice the actuator can be influenced by many factors, such as the drift of the electrical characteristics of the driving circuits, the aging of the mechanical components and etc, so the number of the unknown parameter θ may not be equal to the number of the actuators. However these factors can be reflected by θ, which has a explicit physical meaning: the force generated in a infinitely small time element Δt. The total force generated over a time interval $[0,\tau]$ can be expressed as $\int_0^\tau \theta dt$.

In this paper, we consider the matrix $G(\theta)$ without all-zero rows, which means each degree of freedom is controllable. However the control allocation algorithm designed is not

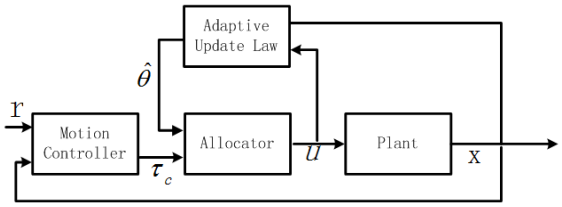

Fig. 1. Structure of adaptive control allocation

limited to this case. When the matrix $G(\theta)$ includes all-zero rows, by performing state transformation $\xi = Tx$, the resulted control effectiveness matrix can be written as:

$$G_r(\theta) = \begin{bmatrix} O \\ G_a(\theta) \end{bmatrix} \tag{3}$$

where G_a is the control effectiveness matrix corresponding to the actuated states, $O = [o_{ij} = 0]$ is a matrix corresponding to the un-actuated states. In this case, when assumption 3 is satisfied, replacing the matrix $G(\theta)$ with $G_a(\theta)$, the control allocation algorithm proposed is still applicable.

Following assumptions are necessary for the adaptive control allocation algorithm presented in this paper:

Assumption I The parameters of effectors varies "slowly" in contrast with the control action of adaptive control allocation algorithm, that is $\dot{\theta} \approx 0$.

Assumption II The control effectiveness matrix can be decomposed to be $G(\theta) = G_s\Lambda(\theta)$, where $\Lambda(\theta) = diag\,(\theta_1 \quad \theta_2 \quad ... \quad \theta_m)$ is a diagonal matrix. $G_s = \{g_{ij}|g_{ij} = \pm 1\}$ is a constant matrix determined by the geometrical layout of the actuators.

Assumption II puts a restriction on the control effectiveness matrix G. In practice, this condition holds for vehicles with fixed actuators due to the definition of the effectiveness matrix (see the example in [10]), the testbed used in the simulation satisfies this condition.

It can be inferred from assumption 2 that $\tau = G_s\Lambda(\theta)u = G_s\Lambda(u)\theta$.

Assumption III There exists a high-level controller such that the nonlinear vehicle (1) is globally stable. The output of the high-level controller is achievable for the reference control allocation algorithm, that is there exists $u \in U$ such that $G(\theta)u = \tau_c$.

Assumption IV The states of the controlled plant are measurable.

III. ADAPTIVE CONTROL ALLOCATION ALGORITHM DESIGN

The diagram of the adaptive control allocation algorithm is as illustrated in figure (1).

In figure (1), the motion controller is a high-level controller that stabilizes the nonlinear system (1). Its output τ_c is the control moment that is distributed to actuators. When the parameters of effectors are known and time-invariant, the reference control moment τ_c can be achieved instantly and precisely if it is feasible. Therefore the nonlinear vehicles (1) is stable accounting for assumption 3. But when the parameters of the effectors drift, the practical control input τ deviates from the given command τ_c thus causes bias of x.

The basic idea of the proposed scheme is to design a nonlinear estimator described by (4), which outputs the estimated value of the parameters as the input of the allocator. The allocator distributed the recommended control moments τ_c to actuators based on the estimated parameters $\hat{\theta}$.

$$\begin{aligned} \dot{\hat{x}} = &\quad f(x,t) + G(\hat{\theta})u - K_x(x - \hat{x}) \\ = &\quad f(x,t) + H(u)\hat{\theta} - K_x(x - \hat{x}) \end{aligned} \tag{4}$$

where $K_x > 0$ is a real number, $\hat{x}$ is the estimation of the state of the controlled plant, $H(u) = G_s\Lambda(u)$. Assumption II is used in 4.

The allocator in Figure 1 aims to solve the following optimization problem:

$$minJ = \|Qs_r\| + \|Wu_r\| \tag{5}$$

subject to

$$\begin{cases} \tau_c - G(\theta_d)u_r = & s_r \\ u_r \in & U \end{cases}$$

This problem has been well studied and many solutions are available (see [6]).

In what follows, an adaptive updating law of the estimated parameters $\hat{\theta}$ is designed such that $\hat{x}$ converges to the actual value of the state vector x, i.e. $\lim_{t\to\infty} \hat{x}(t) = x$. The adaptive updating law of $\hat{\theta}$ is designed as:

$$\dot{\hat{\theta}} = H^T(u)\tilde{x} \tag{6}$$

where $\tilde{x} = x - \hat{x}$ is the error vector.

The overall system with adaptive control allocation algorithm can be concluded as

$$\dot{x} = f(x,t) + H(u)\theta \tag{7}$$

$$\dot{\hat{x}} = f(x,t) + H(u)\hat{\theta} - K_x\tilde{x} \tag{8}$$

$$\dot{\hat{\theta}} = H^T(u)\tilde{x} \tag{9}$$

The theorem below gives conclusion on the stability of the estimator.

Theorem1 The estimated state $\hat{x}$ globally asymptotically converges to the true value of x, with the estimator designed as (4) and the updating law (6) under assumption I, II, IV , when K_x is positive definite and there exists $C_k > 0$ such that $z^T K_x z \leq C_k|z|^2$ for any z.

Note that only the stability of θ can be guaranteed by theorem 1, which will be shown in the following proof. However, the stability of the whole control system can be guaranteed as illustrated by theorem 2.

Proof: Subtracting (8) from (7) yields the dynamical equation of $\tilde{x}$

$$\dot{\tilde{x}} = H(u)(\theta - \hat{\theta}) - K_x\tilde{x} \tag{10}$$

. Define the parameter error $\tilde{\theta} := \theta - \hat{\theta}$, then (10) can be rewritten as

$$\dot{\tilde{x}} = H(u)\tilde{\theta} - K_x\tilde{x}$$

. Differentiating $\tilde{\theta}$ renders $\dot{\tilde{\theta}}$

$$\dot{\tilde{\theta}} = -H^T(u)\tilde{x}$$

where assumption I is used. Then the error system can be concluded as

$$\begin{cases} \dot{\tilde{x}} = & H(u)\tilde{\theta} - K_x\tilde{x} \\ \dot{\tilde{\theta}} = & -H^T(u)\tilde{x} \end{cases} \tag{11}$$

.

Choose a Lyapunov function $V = \frac{1}{2}\tilde{x}^T\tilde{x} + \frac{1}{2}\hat{\theta}^T\hat{\theta}$, its derivative along the trajectory of (11) is

$$\begin{aligned} \dot{V} &= \tilde{x}^T\dot{\tilde{x}} + \tilde{\theta}^T\dot{\tilde{\theta}} \\ &= \tilde{x}^T(-K_x\tilde{x} + H(u)\tilde{\theta}) - \tilde{\theta}^T H(u)\tilde{x} \\ &= \tilde{x}^T(-K_x\tilde{x} + H(u)\tilde{\theta} - H(u)\tilde{\theta}) \\ &= -\tilde{x}^T K_x\tilde{x} \end{aligned}$$

which is negative semidefinite when $K_x > 0$. This renders stability of $[\tilde{x} \quad \tilde{\theta}]^T$. To prove the asymptotic stability of $\tilde{x}$, we need to guarantee that $\ddot{V}$ is bounded. By differentiating $\dot{V}$, one gets

$$\begin{aligned} \ddot{V} =& -(\tilde{x}^T K_x\dot{\tilde{x}} + \dot{\tilde{x}}^T K_x\tilde{x}) \\ =& \tilde{x}^T(K_xK_x + K_x^TK_x)\tilde{x} - \tilde{x}^T K_x H(u_r)\tilde{\theta} - \tilde{\theta}^T H^T(u_r)K_x\tilde{x} \end{aligned} \tag{12}$$

. Since $u \in U$ and $u_r \in U$ are bounded, $z^T K_x z \leq C_k|z|^2$, $\ddot{V}$ is bounded combining with the boundedness of $[\tilde{x} \quad \tilde{\theta}]$. Therefore the asymptotic stability of $\tilde{x}$ is achieved according to Barbara lemma. However this does not lead to the asymptotic stability of $\tilde{\theta}$ for $rank(H(u)) < dim(\hat{\theta})$. Proof completed.

Next the stability of the whole control system will be analyzed. The following theorem gives the result on the stability of the overall close-loop system.

Theorem2 The overall close-loop system composed of (7), (8) and (9) admits globally stability if assumption III holds.

Proof: Replacing $\theta = \hat{\theta} + \tilde{\theta}$ in (7) yields

$$\dot{x} = f(x,t) + H(u)(\hat{\theta} + \tilde{\theta}) \tag{13}$$

$$= f(x,t) + H(u)\hat{\theta} + H(u)\tilde{\theta} \tag{14}$$

. Since $H(u)\hat{\theta} = \tau_c$, the equation above can be furthermore rewritten as

$$\begin{aligned} \dot{x} &= f(x,t) + \tau_c + H(u)\tilde{\theta} \\ &= f(x,t) + \tau_c + \dot{\tilde{x}} + K_x\tilde{x} \\ &= f(x,t) + \tau_c + [I \quad K_x]\begin{bmatrix} \dot{\tilde{x}} \\ \tilde{x} \end{bmatrix} \end{aligned}$$

. (15) can be viewed as a system $\Sigma_1 : \dot{x}_1 = f(x,t) + \tau_c$ cascaded with system Σ_2 : equation (11) by the gain matrix $[I \quad K_x]$. According to the well know cascade theory [8], if system Σ_2 is globally asymptotically stable and Σ_1 is globally stable, the cascade system admits global stability. Assumption III guarantees that Σ_1 is stable, and by theorem 1, $\tilde{x}$ is globally asymptotically stable. The only receipt we need is that $\dot{\tilde{x}}$ is globally asymptotically stable. In fact, this is the case when $\frac{d}{dt}[H(u)\tilde{\theta} - K_x\tilde{x}]$ is uniformly continuous according Barbalat lemma [14]. proof complete.

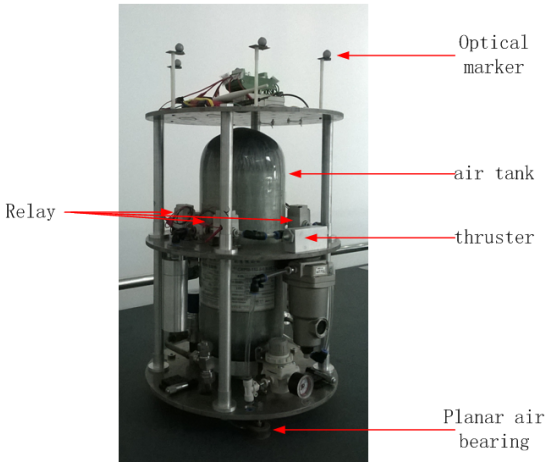

Fig. 2. Structure of the spacecraft simulator

IV. SIMULATION

In this section, the adaptive control allocation algorithm is applied to a planar spacecraft simulator. A path following experiment is designed to test the performance of the adaptive control allocation algorithm. The control objective is to drive the spacecraft simulator to a predefined straight line and thereafter remain there. The negative effects brought by parameter uncertainty of the effectors are exhibited firstly as a reference point. Then the performance of the adaptive control allocation algorithm is illustrated.

The planar spacecraft simulator is an equipment that is used in ground experiment to simulate the manipulation of spacecrafts operating in outer space. The hardware of the simulator is illustrated in figure (2)

The coordinate systems used to describe the dynamics of the spacecraft simulator are illustrated in figure (3), i.e. the inertial frame, the path-fixed frame and the body-fixed frame. As the predefined path is a straight line, which is stationary with respect to the inertial frame, the body-fixed frame and the path-fixed frame are sufficient to describe the dynamics of the spacecraft simulator.

Based on rigid body dynamics, the model of spacecraft simulator is derived as follows, detailed derivation can be found in [11].

$$\begin{bmatrix} \nu_x^b \\ \nu_y^b \\ \omega^r \end{bmatrix} = \begin{bmatrix} cos\psi^r & sin\psi^r & 0 \\ -sin\psi^r & cos\psi^r & 0 \\ 0 & 0 & 1 \end{bmatrix} \begin{bmatrix} \dot{x}^r \\ \dot{y}^r \\ \dot{\psi}^r \end{bmatrix} \tag{15}$$

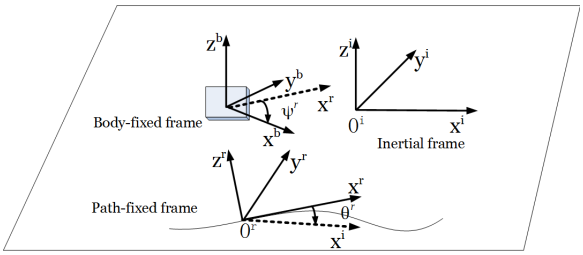

Fig. 3. Coordination systems

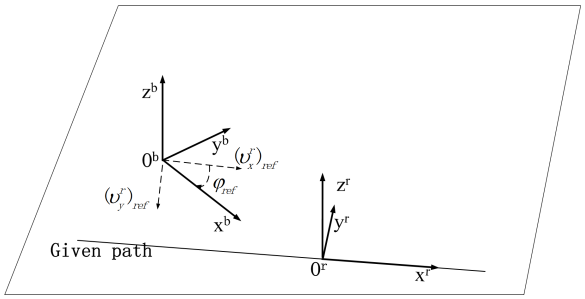

Fig. 4. Geometrical illustration of the reference orientation ψ_r

$$\begin{cases} \dot{\nu_x^b} = \dfrac{1}{m}(m\nu_y^b\omega^r + \tau_1) \\ \dot{\nu_y^b} = -\nu_x^b\omega^r \\ \dot{\omega^r} = \dfrac{1}{J}(\tau_2) \end{cases} \tag{16}$$

where (x^r,y^r) are the position of the spacecraft simulator expressed in the path-fixed frame, ψ^r is the orientation of the spacecraft simulator with respect to the path-fixed frame, ν_x^b and ν_y^b are the velocity coordinates of the spacecraft simulator in the body-fixed frame, τ_1, τ_2 are control moment, i.e. force and torque respectively, $m = 17.2kg$ and $J = 1.03kg \cdot m^2$ are the mass and the moment of inertia of the spacecraft simulator respectively.

The model of the effectors is as

$$\begin{bmatrix} \tau_1 \\ \tau_2 \end{bmatrix} = C(\theta)u \tag{17}$$

where $C(\theta) = \begin{bmatrix} \theta_1 & -\theta_2 & \theta_3 & -\theta_4 \\ -R\theta_1 & R\theta_2 & R\theta_3 & -R\theta_4 \end{bmatrix}$ is the control effectiveness matrix, $u \in R^4$ is the control input of actuators, that is the duty ratio of the driving PWM (Pulse Width Modulation) signal, $u \geq 0$, R is the distance from the point where the thruster act on the body to the vertical symmetric axis of the spacecraft simulator.

The planar spacecraft simulator has 3 variables to control, i.e. (x^r, y^r, ψ^r), while there are four control inputs. Like many practical spacecrafts, the planar spacecraft simulator is a typical over-actuated system.

The model of the simulator (15) and (16) can be expressed in the following compact form:

$$\dot{\chi} = f(\chi) + G_r(\theta)u \tag{18}$$

where $\chi = [x^r \quad y^r \quad \psi^r \quad \nu_y^b \quad \nu_x^b \quad \omega^r]^T$, $G_r(\theta) = \begin{bmatrix} O_{4\times4} \\ G(\theta) \end{bmatrix}$ with $G_\theta = \begin{bmatrix} 1/m & 0 \\ 0 & 1/J \end{bmatrix} C(\theta)$

For $C(\theta)$ can be decomposed as

$$C(\theta) = \begin{bmatrix} 1 & -1 & 1 & -1 \\ -R & R & R & -R \end{bmatrix} \begin{bmatrix} \theta_1 & 0 & 0 & 0 \\ 0 & \theta_2 & 0 & 0 \\ 0 & 0 & \theta_3 & 0 \\ 0 & 0 & 0 & \theta_4 \end{bmatrix}$$

, assumption 2 holds true for $G(\theta)$.

To satisfy assumption 4, a high-level motion controller that stabilizes the overall system is designed.

Borrowing the basic idea from [5], the control moment τ_1 is designed as :

$$\tau_1 = -k_1(\nu_x^b - (\nu_x^b)_{ref}) + m(\dot{\nu}_x^b)_{ref} - m\nu_y^b\omega^r \tag{19}$$

where $k_1 > 0$ is a positive constant, $(\nu_x^b)_{ref}$ is the reference velocity along the x-axis of the body-fixed frame, which is given by (see figure 4 for the geometric explanation):

$$(\nu_x^b)_{ref} = \sqrt{(\nu_x^r)_{ref}^2 + (\nu_y^r)_{ref}^2} \tag{20}$$

being $(\nu_x^r)_{ref} = c$ a predefined constant velocity, and $(\nu_y^r)_{ref}) = -k_4 y^r$ the given velocity along the y-axis direction of the path-fixed frame.

The other control moment τ_2 is designed to stabilize the orientation loop.

$$\tau_2 = -k_2(\omega^r - \omega_{ref}^r) - k_3(\psi^r - \psi_{ref}^r) + J\dot{\omega}_{ref}^r \tag{21}$$

where the reference orientation ψ_{ref}^r (see figure 4) is given as

$$\psi_{ref}^r = tan^{-1}(\frac{(\nu_y^r)_{ref}}{(\nu_x^r)_{ref}}) = tan^{-1}(\frac{-k_4 y^r}{c}) \tag{22}$$

.

Differentiating ψ_{ref}^r with respect to time in conjunction with equation (15), we get the reference angular velocity ω_{ref}^r as

$$\omega_{ref}^r = \frac{-k_4(\nu_y^r)_{ref}^2}{(\nu_x^r)_{ref}^2 + (\nu_y^r)_{ref}^2}(\nu_x^b sin(\psi^r) + \nu_y^b cos(\psi^r)) \tag{23}$$

The stability analysis can be accomplished by applying the cascade system theory. It is not the emphasis of this paper and therefore not be given here.

Next the digital simulation are implemented to illustrate the performance of the adaptive control allocation algorithm. A instance where the parameters vary slowly while non-adaptive control allocation algorithm (direct allocation algorithms regardless of parameter uncertainty) is taken as the reference point. The nominal value of parameter $\theta_i = 1.8, i = 1, 2, 3, 4$ and is assumed to be constant.

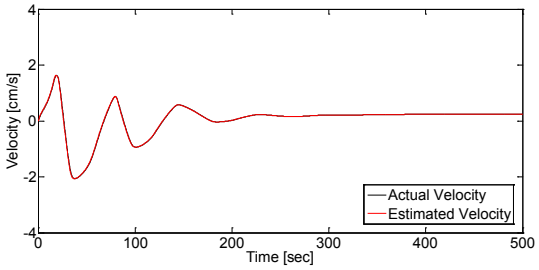

Fig. 5. The comparison of ν_x^b and $\hat{\nu}_x^b$

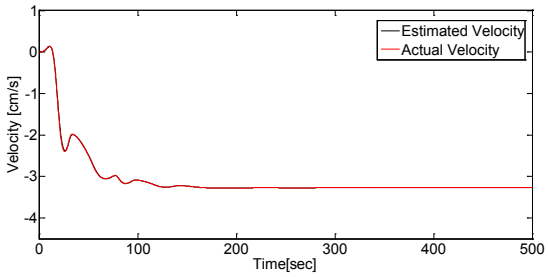

Fig. 6. The comparison of ν_y^b and $\hat{\nu}_y^b$

In the digital simulation, a slowly varying vector $\begin{bmatrix} \theta_1(t) \\ \theta_2(t) \\ \theta_3(t) \\ \theta_4(t) \end{bmatrix} = \begin{bmatrix} 2[1+0.1sin(0.1t)] \\ 1.9[1+0.1sin(0.1t+2)] \\ 1.7[1+0.1sin(0.1t+9)] \\ 1.8[1+0.1sin(0.1t+10)] \end{bmatrix}$ is used as the practical parameter vector.

The given path is a straight line $y_{ref}^r = 0$, the initial position is $\begin{bmatrix} x^r(0) \\ y^r(0) \end{bmatrix} = \begin{bmatrix} 0 \\ -10 \end{bmatrix}$, the commanded velocity along the given path is $0.02m/s$, the given orientation is $\psi^r = 0$.

The parameters of the controller are designed as $k_1 = 0.2, k_2 = 0.2, k_3 = 0.2, k_4 = 0.45$. Observing the structure of $G_r(\theta)$ in (18), it can be seen that $\hat{\theta}$ depends only on ν_x^b and ω^r, so we choose $\hat{x} = [\hat{\nu}_x^b \quad \hat{\nu}_y^b \quad \hat{\omega}^r]^T$, and design $K_x = \begin{bmatrix} 0.9 & 0 & 0 \\ 0 & 0.5 & 0 \\ 0 & 0 & 0.7 \end{bmatrix}$.

Figure 5, 6 and 7 illustrate the comparison of $\nu_x^b, \nu_y^b, \omega^r$ and the corresponding estimated variables. From figure 5, 6 and 7, it can be easily seen that the error between the estimated state and the actual state $\begin{bmatrix} \nu_x^b - \hat{\nu}_x^b \\ \nu_y^b - \hat{\nu}_y^b \\ \omega^r - \hat{\omega}^r \end{bmatrix}$ tends to zero rapidly. This validates the correctness of theorem 1. Figure 8 shows the time evolution of the estimated parameters. It can be seen that the estimated parameters are not equal to the corresponding true values, which verifies the conclusion of theorem 1.

Part of intermediate variables are given to show the effectiveness of the adaptive control allocation algorithm. Figure

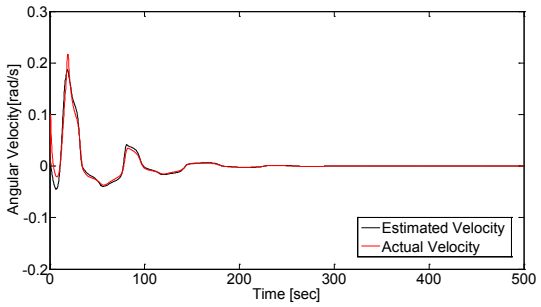

Fig. 7. The comparison of ω^r and $\hat{\omega}^r$

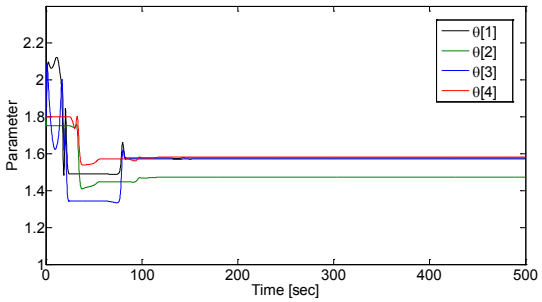

Fig. 8. The comparison of ω^r and $\hat{\omega}^r$

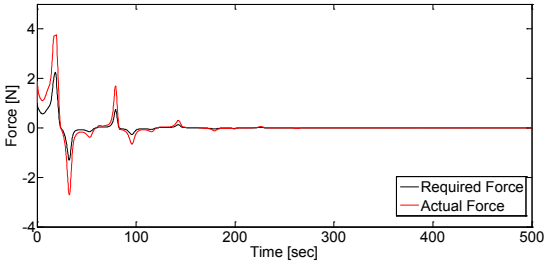

Fig. 9. The force response with the adaptive control allocation algorithm

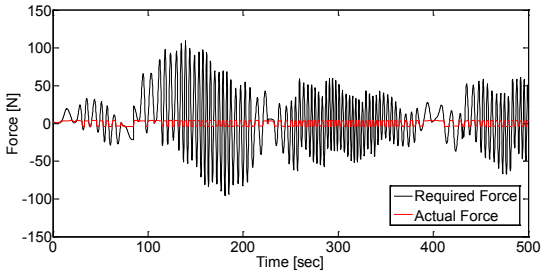

Fig. 10. The force response without the adaptive control allocation

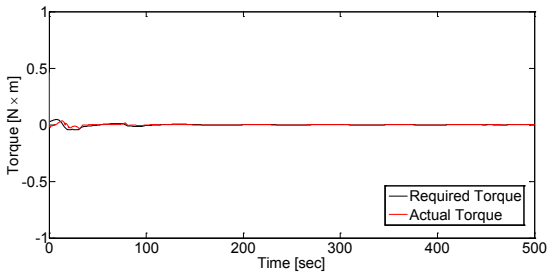

Fig. 11. The torque response with the adaptive control allocation algorithm

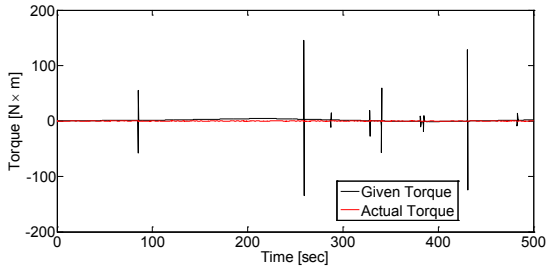

Fig. 12. The torque response without the adaptive control allocation algorithm

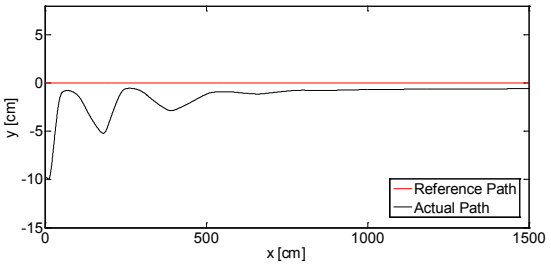

Fig. 13. The path following performance with adaptive control allocation algorithm

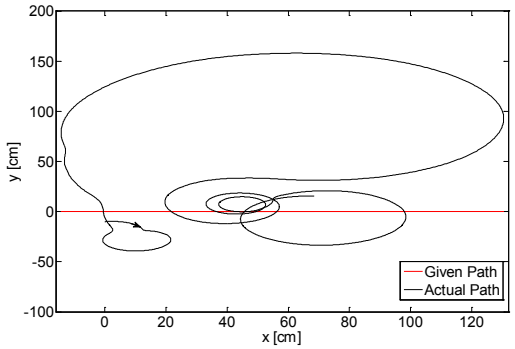

Fig. 14. The path following performance without adaptive control allocation algorithm

9 and 10, 11 and 12 illustrate the comparison of the force response and torque response respectively. Both the force and torque responses are improved drastically when the adaptive control allocation is applied. Figure 13 and 14 compares the path following performance. The path following performance is improved tremendously with the adoption of the adaptive control allocation algorithm. Figure 13 shows a static bias exists for the path following error, this is caused by the high-level controller, for only stability is achieved for the whole system as proved by theorem 2. Without the adaptive control allocation algorithm, the path following performance deviates when the parameter varies, as shown in figure 14.

V. CONCLUSIONS

In this paper, an adaptive control allocation algorithm is designed for nonlinear vehicles with parameter uncertainty and variation. Theoretical analysis is given to prove the stability of the whole control system with the control allocation algorithm. Digital simulation is implemented to validate the effectiveness of the algorithm.

In future works, the adaptive control allocation algorithm will be extended to nonlinear effectors with parameter uncertainty, with the dynamics of the actuator is considered.

REFERENCES

[1] Miller, Christopher J., and Dan Goodrick. "Optimal Control Allocation with Load Sensor Feedback for Active Load Suppression, Flight-Test Performance." 2017.

[2] Cristofaro, Andrea, and Tor Arne Johansen. "Fault tolerant control allocation using unknown input observers." Automatica 50, no. 7: 1891-1897, 2014

[3] Baldi, P., Mogens Blanke, P. Castaldi, N. Mimmo, and S. Simani. "Adaptive FTC based on control allocation and fault accommodation for satellite reaction wheels." In Control and Fault-Tolerant Systems (SysTol), 2016 3rd Conference on, pp. 672-677. IEEE, 2016.

[4] Frost, Susan A., Marc Bodson, John J. Burken, Christine V. Jutte, Brian R. Taylor, and Khanh V. Trinh. "Flight control with optimal control allocation incorporating structural load feedback." Journal of Aerospace Information Systems 12, no. 12 : 825-834, 2015

[5] Moe, Signe, Walter Caharija, Kristin Y. Pettersen, and Ingrid Schjolberg. "Path following of underactuated marine surface vessels in the presence of unknown ocean currents." In American Control Conference (ACC), 2014, pp. 3856-3861. IEEE, 2014.

[6] Johansen, Tor A., and Thor I. Fossen. "Control allocation - a survey." Automatica 49, no. 5 : 1087-1103, 2013

[7] Page, Anthony, and Marc Steinberg. "A closed-loop comparison of control allocation methods." In AIAA Guidance, navigation, and Control Conference and Exhibit, p. 4538, 2000.

[8] Tjnns, Johannes, and Tor A. Johansen. "Adaptive control allocation." Automatica 44, no. 11 : 2754-2765, 2008

[9] Fossen, Thor I. Handbook of marine craft hydrodynamics and motion control. John Wiley & Sons, 2011.

[10] Wang, Min, and Yongchun Xie. "Design of the optimal thruster combinations table for the real time control allocation of spacecraft thrusters." In Decision and Control, 2009 held jointly with the 2009 28th Chinese Control Conference. CDC/CCC 2009. Proceedings of the 48th IEEE Conference on, pp. 5063-5068. IEEE, 2009.

[11] Chobotov, Vladimir A. "Spacecraft attitude dynamics and control." NASA STI/Recon Technical Report A 92, 1991.

[12] Guo-Ping, L. I. U., Sun Jian, and Z. H. A. O. Yun-Bo. "Design, analysis and real-time implementation of networked predictive control systems." Acta Automatica Sinica 39, no. 11 (2013): 1769-1777.

[13] Chen, Dongliang, and Guoping Liu. "A real-time Networked Control framework based on mobile phones." In Mechatronics and Automation (ICMA), 2015 IEEE International Conference on, pp. 1772-1778. IEEE, 2015.

[14] Khalil, H. K. (1996). Noninear Systems. Prentice-Hall, New Jersey, 322-329.